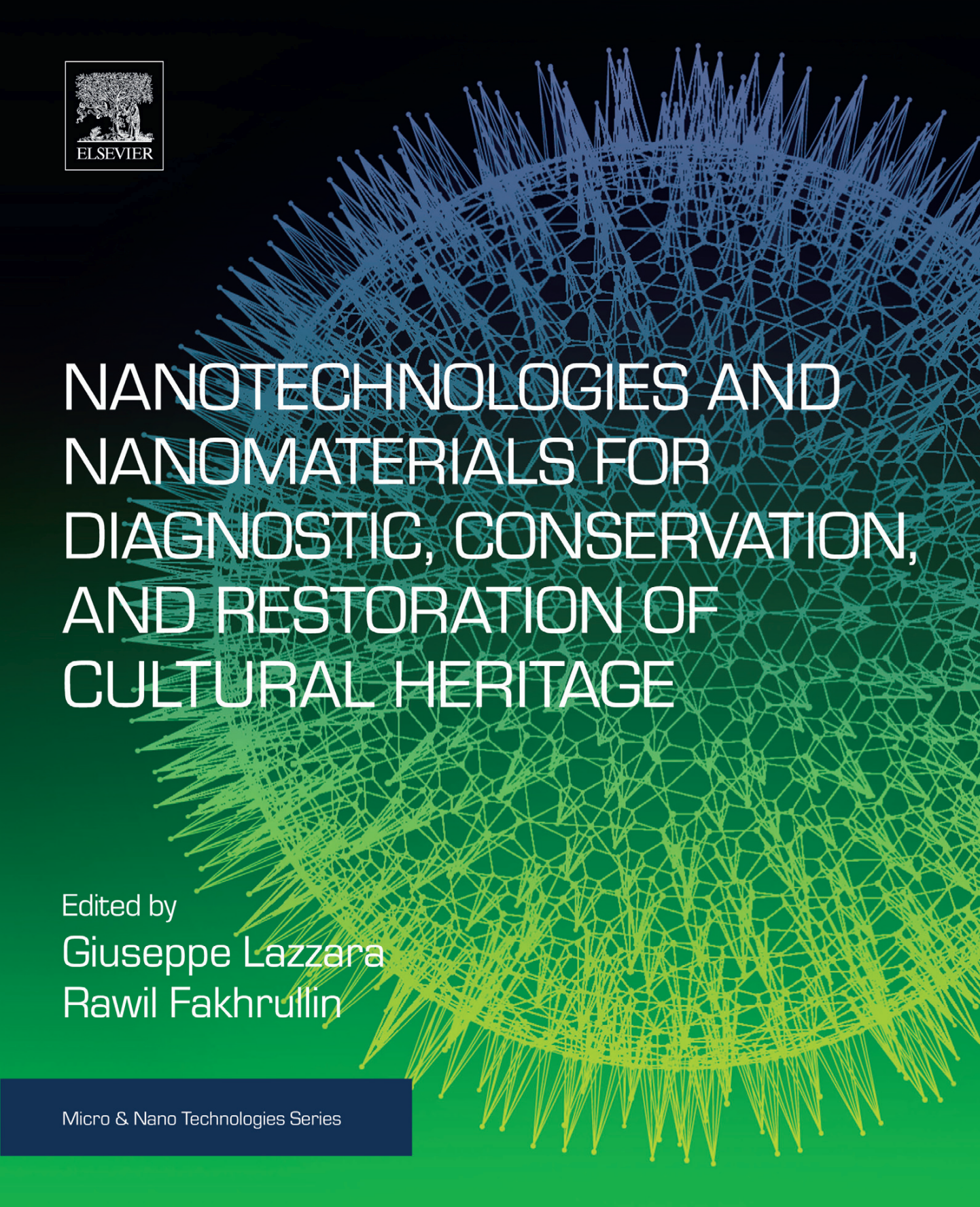
ELSEVIER
NANOTECHNOLOGIES AND NANOMATERIALS FOR DIAGNOSTIC, CONSERVATION, AND RESTORATION OF CULTURAL HERITAGE
Edited by
Giuseppe Lazzara
Rawil Fakhrullin
Micro & Nano Technologies Series

CHAPTER 10

Ancient and Modern Binders: Naturally Nanostructured Materials

Michele Secco[1,2], **Luca Valentini**[2,3], **Anna Addis**[3]

[1]University of Padova, Department of Civil, Environmental and Architectural Engineering (ICEA), Padova, Italy; [2]University of Padova, Inter-Departmental Research Center for the Study of Cement Materials and Hydraulic Binders (CIRCe), Padova, Italy; [3]University of Padova, Department of Geosciences, Padova, Italy

Chapter Outline

10.1 Introduction

Among the various geomaterials developed during the technological evolution of human knowledge, inorganic binders are so far the ones that experienced the earliest chronological development, associated with a marked empirical attention toward the exploitation of nanotechnology to tailor and optimize the final properties of the produced artifacts. The first evidence of human utilization of inorganic materials with chemical-physical binding properties can be found in the parietal wall paintings of the Altamira and Lascaux caves, dated back to the upper Paleolithic, 16,500 BC, where figurative scenes

Nanotechnologies and Nanomaterials for Diagnostic, Conservation, and Restoration of Cultural Heritage. https://doi.org/10.1016/B978-0-12-813910-3.00010-0

were depicted employing ochre pigments bound to the stone exploiting the cohesive properties of nanostructured clay minerals. The introduction of pyrotechnology constituted a turning point for the evolution of inorganic binders, from that moment on produced through anthropogenic processes capable of modifying their chemical-physical properties and optimizing their cohesive performances. The first evidence of utilization of a pyrotechnology-derived inorganic binder dated back to the Epi-Paleolithic period (approximately 12,000 BC) in the Levant region, as a lime-based adhesive to assemble a tool from flint microliths in the Geometric Kebaran site Lagama North VIII (Bar-Yosef and Goring-Morris, 1977). Early employment of lime-based materials for plastering and flooring purposes were found in the same region, as in the Hayonim Cave, 10,400−10,000 BC (Bar-Yosef, 1983) and Catal Huyuk site, 9000 BC (Stark and Wicht, 1999), as well as in other geographical areas, like the Lepenski Vir site, Serbia, dated back to 5600 BC (Bensted, 1997). The nanostructured nature of such early binders is clearly evident, being generally constituted by submicrometric spherulites of anthropogenic calcium carbonate (Kingery et al., 1988).

The utilization of inorganic binders experienced a widespread diffusion among the great Bronze age urban civilizations of the Near East and North Africa, such as the Sumerians-Akkadians and the Ancient Egyptians. Early evidence of the utilization of mortar in Mesopotamia dated back to 5000−4000 BC, while the first permanently established lime kilns dated back to 2000 BC (Schiele and Berens, 1976). On the other hand, Ancient Egyptian culture, gypsum-based binders were used in place of lime, both for plastering and structural purposes (Pecchioni et al., 2008).

Later, the utilization of inorganic binders was widely applied by the Mediterranean civilizations of the second and first millennium BC, like the Phoenician-Punic and Minoan ones. These cultures contributed to a relevant technological evolution in the field of inorganic binders through the introduction of the so-called pozzolanic additions, fine powders of siliceous compounds, mainly *cocciopesto* (Bensted and Coleman, 2004) and combustion ashes (Lancaster, 2012), capable of reacting with lime and precipitate nanostructurally polymerized insoluble silicate phases with excellent mechanical, permeability, and durability properties. Such traditions were assimilated by the Greek culture, but only marginally used for architectural purposes, mainly for nonstructural plastering (Pecchioni et al., 2008), while the potentialities of lime-based binders were fully experimented in the Roman world.

Starting from the Greek technological background, mediated through the Etruscan culture, the Ancient Romans had the intuition to comprehend the enormous potentialities related to the application of inorganic binders for large-scale structural purposes, introducing their utilization in architecture at the end of the third century BC (Cagnana, 2000; Collepardi, 2003) through the formulation and development of Roman concrete, *opus caementicium*

(in Latin). Composed of extremely reactive calcic limes, pozzolanic additions of various natures, and coarse aggregates, such material fully demonstrates the ability of ancient Romans to learn from the past traditions, pushing the properties of the resulting composite material through a thorough optimization the chemical, physical, and textural properties of the single constituents and their resulting mixes. Apart from the invention of this revolutionary construction material, the ancient Romans gave crucial importance to the parametrization of the production techniques of their binders, through the writing of several codes of practice for the selection of the raw materials, optimization of the production processes, and definition of standard mixes and building procedures. The first written source related to the definition of a technological procedure related to the production of inorganic binders can be found in the *Liber De Agri Cultura* of Cato the Elder (160 BC), where a thorough description of a lime kiln can be found. Later, Marcus Vitruvius Pollio, between 30 and 15 BC, wrote the most comprehensive encyclopedia of construction techniques of Roman times, the Ten Books of Architecture (*De Architectura*), followed by the Natural History (*Naturalis Historia*) of Pliny the Elder, written between AD 77 and 79. Such manuals report astonishingly detailed prescriptions both for materials and building practices in the Roman world, and their accuracy fully justifies the marked architectural quality and standardization that can be observed even in present times on the abundant remnants of Roman buildings all around Europe and the Mediterranean regions.

Such pioneering globalization of the construction practices rapidly disappeared with the fall of the Roman Empire in the 5th century AD, leading to a steep decline in the quality of materials and construction techniques during the Middle Ages. A progressive reestablishment of the advanced Roman construction techniques took place from the 15th century AD on, thanks to the rediscovering of the works of Vitruvius and Pliny, which influenced all the construction practices of the Renaissance.

The next big technological advance took place during the Industrial Revolution, with the introduction of hydraulic binders. Moving away from the Roman prescriptions, based on pure calcic systems, in 1793 John Smeaton produced a lime obtained by the calcination of marls, capable of setting and hardening under water. This hydraulic lime is considered the progenitor of Portland cement, patented by William and Joseph Aspdin in 1824 and obtained by thermal treatment at 850°C of a mixture of limestone and clay. Such revolutionary materials were characterized from the beginning by marked hydraulic properties, like resistance to dissolution under the action of water, related to the formation of nanostructured hydrated calcium aluminosilicates during the reaction process. Their excellent performances led to the development of several scientific studies for the understanding and optimization of their properties (Barbisan and Guardini, 2007). After these pioneering studies, the use of hydraulic binders became widespread in the construction technology field both in Europe and the United States. A further step in the evolution of cement production technology was the introduction of rotary kilns at the end

of the 19th century, which were able to produce cements with compositional characteristics and properties fully comparable to modern binders (Barbisan and Guardini, 2007).

The latest evolutions in the field of modern hydraulic binders came in the introduction of nanostructured chemical admixtures, both organic and inorganic, capable of modifying the material properties both at fresh and hardened states. Nowadays, the utilization of such new classes of compounds, together with the optimization of mix designs and the conception of a new generation of sustainable materials, is contributing to a further optimization of the performances in terms of both mechanical properties and durability, enhancing the crucial role of inorganic binders in contemporary building technology.

In the next paragraphs, several detailed aspects of the technological evolution of inorganic binders over time will be deepened, with particular attention to the influence of naturally and artificially induced nanostructuring of particles on the optimization of the physical and chemical properties of both ancient and modern binding compounds.

10.2 Ancient Lime Binders: Tailoring the Reactivity Through Empirical Nanostructural Optimization

Among the several inorganic binders formulated during the history of humankind, lime is by far the most widely employed, especially in the architectural field. The success of such a geomaterial is clearly demonstrated by the preservation of several archaeological remnants of human structures since the Epi-Paleolithic period, with numerous cases of buildings and infrastructures still in perfect functional condition, especially from the ones related to the Roman period.

The excellent properties of lime, both in terms of mechanical strength and durability, are mainly related to its adhesive properties to the masonry units, but also to its plastic deformation ability, high porosity and permeability, and water retentivity (Cizer, 2016). All these characteristics contribute to the elasto-plastic failure behavior under stress due to a pore collapse mechanism, and thus allow masonry to gain a better ability to adapt to differential settlements, increasing at the same time mechanical performances and durability (Hansen et al., 2008).

Research on ancient lime mortars allows a better investigation of the crucial factors for the long-lasting durability of such materials, and several studies proved the crucial role of the colloidal and nanostructural characteristics of both fresh lime and hardened anthropogenic carbonates. Such characteristics have been obtained since ancient times through a careful empirical optimization of the whole reaction process, from the quarrying of the raw material to the final hardening of the lime-based binders. The several stages of lime production and utilization are strongly correlated through the so-called lime cycle, which leads to a final product, $CaCO_3$ in several polymorphs, chemically equivalent to the

starting limestone raw material (Cizer, 2016). The production stages of lime start with the calcination of pure limestones at temperatures generally between 700 and 900°C, which allow a decomposition of the original calcium carbonate with the formation of calcium oxide (CaO, also defined as quicklime) and the release of CO_2. The widespread diffusion of such a production process even in prehistoric times is mainly related to the fact that such temperatures are easily reachable even through burning of standard wood. The obtained quicklime, highly metastable, is then subjected to a forced hydration process called slaking, through the submersion and aspersion of water, obtaining calcium hydroxide ($Ca(OH)_2$, also defined as portlandite), which is the mineral constituent of lime. The amount of water should be either stoichiometric, obtaining a powder of hydrated lime, or in excess, obtaining a slurry called lime putty. Such a compound subsequently reacts with atmospheric CO_2, forming anthropogenic calcium carbonate crystals through the following simplified carbonation reaction:

$$Ca(OH)_2 + CO_2 + H_2O \rightarrow CaCO_3 + 2H_2O \tag{10.1}$$

Such a reaction process is actually controlled by diffusion-related factors and by the low concentration of carbon dioxide in the atmosphere, so lime mortar carbonation generally proceeds gradually, according to an interfacial process and only after an initial dormant phase during which a partial drying occurs until reaching relative humidity values between 40% and 80%, necessary to start CO_2 diffusion and dissolution within the partially filled pore network of the material (Cizer, 2016).

According to these factors, the carbonation process can be subdivided into different reaction steps, namely dissolution of CO_2 into the aqueous medium (Eq. 10.2), interaction of CO_2 with hydroxyl ions to form bicarbonate and carbonate ions (Eqs. 10.3 and 10.4), and final reaction of the carbonate ions with Ca^{2+} (Eq. 10.5) (Cizer, 2016):

$$CO_{2(g)} \leftrightarrow CO_{2(aq)}; \tag{10.2}$$

$$CO_{2(aq)} + OH^-_{(aq)} \leftrightarrow HCO_3^-{}_{(aq)}; \tag{10.3}$$

$$HCO_3^{-(aq)} + OH^-{}_{(aq)}CO_3^{2-}{}_{(aq)} \leftrightarrow \ + H_2O_{(l)}; \tag{10.4}$$

$$Ca^{2+}{}_{(aq)} + CO_3^{2-}{}_{(aq)} \leftrightarrow CaCO_{3(s)}. \tag{10.5}$$

In the proposed array of chemical reactions, Eq. 10.3 is the rate-controlling step, being slower with respect to Eq. 10.4, which is practically instantaneous. Starting from the proposed carbonation model, an experimental study (Cizer et al., 2012) proved that lime carbonation proceeds in three stages. Stage I proceeds under a chemical-reaction controlled regime due to the limited CO_2 diffusion through the saturated pore network. Furthermore, the initial CO_2 uptake promotes a rapid carbonation on the surfaces of

portlandite crystals, forming a passivating layer of amorphous $CaCO_3$ that facilitates the instauration of a dormant period. The reactivation of the carbonation process, which proceeds rapidly during stage II, is promoted both by the conversion of amorphous calcium carbonate into calcite and by the drying effect, which favors the diffusion of CO_2 within the system. Such a stage is strictly diffusion controlled. The final stage III takes place after the completion of the surface carbonation, with the transition to a diffusion-controlled regime significantly hindered by the reduced permeability of the carbonated layer. Furthermore, the study demonstrated that the reaction rate and the amount of CO_2 uptake are not proportional to the initial CO_2 concentration, but they are more influenced by the crystallographic and dimensional characteristics of lime. More in detail, the smaller the particles of portlandite, the faster the transition from stage I to stage II due to their higher solubility and consequent reaching of higher levels of supersaturation during the chemical reaction processes, leading to a higher nucleation density of the calcite crystals.

Such experimental evidence has direct consequences in the determination of the production stages to optimize in the framework of lime cycle, in order to obtain better nanostructured, and thus more reactive, calcic limes. The two stages that allow higher operative margins are the calcination and the slaking processes, and the analysis of both archaeological materials and written sources undoubtedly confirmed that the ancient technological protocols took empirically into account such parameters in order to boost the properties of the obtained limes.

As for the calcination process, the *Liber De Agri Cultura* of Cato the Elder gives detailed prescriptions on the layout and dimensions of lime kilns, on the techniques to seal the internal chamber from the external environment in order to favor the circulation of heat and gases, and on the procedure for the charging of raw materials (Catone, 2000). All these prescriptions are clearly addressed toward a thorough and standardized optimization of the firing temperature. According to the type of prescribed fuel (wood) and the characteristics of the kiln itself, it should be between 850 and 900°C. The physical-chemical implications of such a thoroughly optimized production process, besides reaching temperatures higher than the calcination temperature of calcium carbonate, have been investigated by scientific studies. An experimental study by Moropolou and coauthors (Moropoulou et al., 2001), consisting of experimental calcination processes at increasing temperatures on two different types of Cretan limestones, demonstrated that the best quicklime reactivity is obtained through the adoption of firing temperatures around 900°C, with a progressive loss of reactivity at increasing values. In more detail, the samples calcined at 900°C are characterized by a higher total cumulative volume, porosity, and specific surface area, measured through mercury intrusion porosimetry and nitrogen absorption. Furthermore, they are characterized by higher temperature increase and higher expansion during slaking.

A more detailed experimental study (Rodriguez-Navarro et al., 2009), employing advanced analytical techniques like field emission scanning electron microscopy (FESEM), two-dimensional X-ray diffraction (2DXRD), and transmission electron microscopy coupled with selected area electron diffraction (TEMSAED), unveiled more detailed mineralogical insights on the factors influencing such increased reactivity besides demonstrating the nanostructural arrangement of quicklime particles during and after firing. First, the study indicated that the temperature transformations are independent on the experimental conditions as carbon dioxide partial pressure, calcite crystal size, and type of energy used to activate the decomposition reaction, further indicating that the adopted temperature is the driving force for the reaction path of the thermal process during calcination. Furthermore, the experimental evidence clearly indicated that the thermal decomposition process of calcium carbonate into calcium oxide is pseudomorphic and topotactic, starting with the formation of a mesoporous structure of oriented rod-shaped CaO nanocrystals on each rhombohedral cleavage face of the calcite pseudomorph. With the progression of the calcination reaction, a collapse of the mesoporous structure occurs, resulting in the oriented aggregation of metastable CaO nanocrystals still within the former rhombohedral calcite microstructural site, with a mean thickness of 5 nm and aggregated in clusters of 1 μm mean cross section. The reaction starts at 600°C with the superficial formation of pockets of oriented CaO crystals, and reaches a full conversion at 850°C. At higher temperatures, relevant sintering phenomena of the CaO crystals take place, with the development at 1000°C of equidimensional, micrometer-sized CaO grains characterized by the occurrence of straight triple boundaries as well as neck contacts, typical features of the sintering process (Kingery, 1960). Concerning the specific surface area, measured by means of nitrogen absorption, highest values were obtained at 750°C, with a progressive reduction at higher temperatures, indicating a reduced triggering of the sintering processes even at values lower than 1000°C. As for the porosity, values close to the theoretical maximum of 54.2% were yielded at 900°C, with a progressive decrease at higher temperatures, clearly indicating an association of sintering and shrinking processes (McClellan and Eades, 1970). Microstructural analyses on calcination relicts of ancient Roman mortars undoubtedly demonstrated the validity of the proposed models, especially regarding the topotactic and pseudomorphic nature of the calcination process and the influence of sintering phenomena on lime reactivity (Fig. 10.1).

On a general basis, the best temperature interval in terms of calcination progression, specific surface area, overall porosity, and prevention of sintering phenomena is between 850 and 900°C, clearly indicating that the empirical determinations of the proper firing temperatures in ancient times are strongly corroborated by modern scientific data.

Concerning the optimization of the slaking process, Chapter 2 of the Seventh book of Vitruvius' *De Architectura* is devoted to the proper procedure for lime aging in excess water in order to obtain a high quality slaked lime. The author suggests putting quicklime

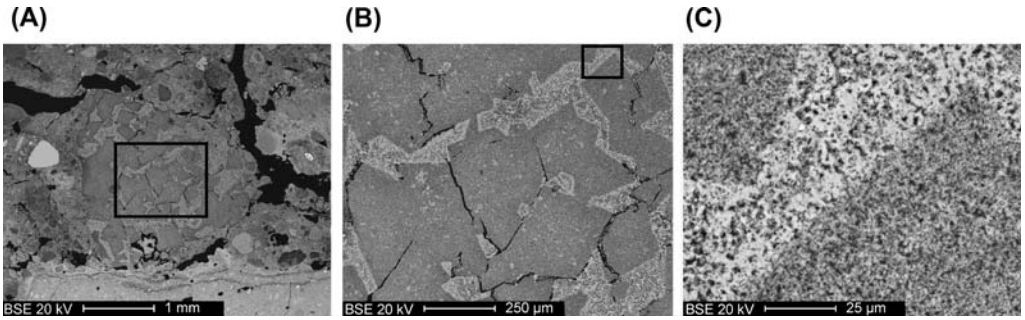

Figure 10.1
Roman flooring concrete from the *Domus di Tito Macro* (Aquileia, North-Eastern Italy, 1st century BC): calcination relict showing the pseudomorphic growth of CaO crystals after the decomposition of large rhombohedral calcite crystals (A and B). The CaO crystals underwent total carbonation upon aging, indicating a proper calcination temperature without relevant sintering phenomena of the CaO crystals (C).

in a pit under water and letting it macerate for a proper amount of time with periodic stirring until obtaining a homogeneous silky dispersion of particles, without any detectable solid lump and with a level of cohesion of the paste allowing it to stick to a hoe submerged inside the pit (Vitruvio, 1997). Concerning the same topic, Plinius the Elder in the Fifth Book of *Naturalis Historia* suggests a slaking time of 3 years to obtain a binder with adequate properties at fresh and hardened states (Plinio il Vecchio, 1984). Several experimental scientific studies investigated the microstructural reasons for such a long preparation (Rodriguez-Navarro et al., 1998; Cazalla et al., 2000; Margalha et al., 2013), demonstrating a clear decrease in portlandite crystallinity upon aging, contributing to a general surface area increase.

From a crystallographic point of view, this is due to a progressive transition from large micrometric prismatic portlandite crystals to hexagonal plate-like, submicrometric ones. Such crystals are characterized by a development parallel to (0001) planes, with a progressive increase of corrosion features on the original prismatic faces along the (0001) cleavage planes and a growth of the $\{0001\}$ faces at the expense of the $\{10\bar{1}0\}$ and $\{10\bar{1}1\}$ ones. The preferential development of the basal faces is evident comparing XRD patterns of standard hydrated limes with the ones of aged slaked putties (Fig. 10.2). This experimental evidence is in contrast with the generally accepted Ostwald ripening theory (Ostwald, 1900); that is, development of larger crystals at the expense of smaller ones to attain the lowest total surface energy of the system. The authors justified this phenomenon taking into account a preferential dissolution of prismatic $\{10\bar{1}0\}$ faces of the large portlandite crystals due to a higher surface energy with respect to the basal pinacoid ones,

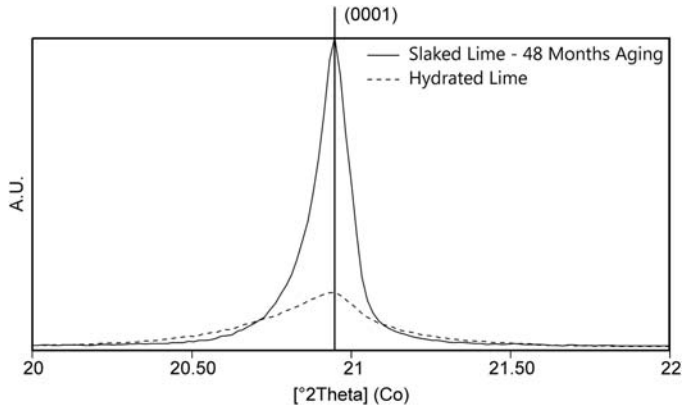

Figure 10.2

Comparison between $Ca(OH)_2$ (0001) planes diffraction peaks of a 48-months-aged slaked lime putty and a commercial hydrated lime powder. The higher intensity observed for the peaks of the slaked lime putty indicates a preferential development of the basal faces upon aging.

facilitating the development of {0001} faces upon aging. This is strictly related to the crystal structure of calcium hydroxide, constituted of layers of $Ca(OH)_2$ having hexagonal symmetry, bonded together by weak van del Waals forces, resulting in a perfect basal cleavage (Hansen et al., 2008).

The observed reduction in particle size and peculiar shapes have direct consequences on the rheological properties of fresh putties and mortars, as demonstrated by several studies (Ruiz-Agudo and Rodriguez-Navarro, 2010; Bohac and Necas, 2016), namely a net plasticity increment due to a greater capacity to absorb water, a higher thixotropic behavior, and a yield stress increment. As for the hardening behavior, an experimental study on several mortars prepared with lime putties aged up to 14 years (Cazalla et al., 2000) demonstrated a faster overall carbonation for the materials prepared with the most aged binders, with a development of smaller crystals of anthropogenic calcite, more interlocked and arranged on a rigid, three-dimensional structure. Furthermore, the binding matrices produced by carbonation of the aged putties show peculiar microstructural features of alternating calcite-rich and portlandite-rich rings, similar to the so-called Liesegang rings forming on far-from-equilibrium precipitating systems (Stern, 1954). Such a precipitation process could be explained considering a fast dissolution of portlandite crystals in the carbonate-saturated solution, due to their higher solubility related to the reduced crystal size. This results in a quick supersaturation with respect to calcium carbonate in the pore solution, followed by rapid calcite precipitation, ion diffusion, and solution mass transport from the saturated surrounding areas toward the precipitation front where reactive concentration depletion occurs. This causes the formation of a thick

external calcite ring surrounding an internal portlandite ring almost dry and with very high pH, preventing further carbonation. Furthermore, the local water evaporation caused by the exothermic carbonation process stops the carbonation in the area of precipitation, causing diffusion of CO_2 toward an inner zone characterized by a proper amount of reactive aqueous solution and thus reactivation of the self-limiting carbonation process (Moorehead, 1985). The progression of this diffusive-precipitating system toward the inner portions of the carbonating paste causes the formation of the aforementioned Liesegang rings. On the contrary, nonaged lime putties with large portlandite crystals of lower solubility are characterized by limited calcite precipitation at low supersaturation ratios, typical for closer-to-equilibrium diffusion-limited systems. In this case, the carbonation process is gradual and homogeneous from the surface toward the sample core.

A more recent study (Mascolo et al., 2010) shed a different light on the crystallographic evolution of lime putty upon aging. Lime putties aged up to 66 months were characterized by means of thermal analyses to determine the initial composition, scanning electron microscopy for particle morphology, mercury intrusion porosimetry for pore size distribution, and static laser scattering for particle size distribution. Results indicated that the aging process produced a significant broadening of the particle size distribution, with an increment not only toward the smaller grain sizes, but also toward the higher ones. Furthermore, the average particle size has a bell shape, showing an increase with a maximum at about 36 months followed by a decrease, and such parameter is inversely correlated with the water retention capacity of the putties, showing a minimum between 24 and 36 months. Such experimental evidences are in accordance with the Ostwald ripening theory, demonstrating that a model hypothesizing a sole development of plate-like portlandite crystals after large prismatic crystals, implying a cutting of the original crystal along the c-axis to form separated thin plates of portlandite, causes a net increment of the total surface energy; thus it is thermodynamically unfavorable. The proposed alternative model hypothesizes the formation of large plate-like crystals after smaller prismatic crystals in accordance with the Ostwald ripening theory, with a subsequent formation of submicrometer plate-like crystals after dissolution of the prism faces of the larger ones due to differences in solubility, as hypothesized by Rodriguez-Navarro et al. (1998). Furthermore, an additional precipitation of submicrometer portlandite crystals could occur after precipitation from aqueous solution due to the seeding effect of the larger particles (Tomazic et al., 1986).

Apart from the correct interpretative model for the evolution of the lime putty over time, such studies clearly demonstrated the great importance given by the ancient Romans to the optimization processes of lime production. The final material was a true nanoengineered product, capable of giving final properties at the fresh and hardened state definitely superior with respect to the standard products produced nowadays.

10.3 Ancient Pozzolanic Binders: Nanostructured Silicates Enhancing the Durability of Masonry

The mixing between lime and natural amorphous silicates, as a method for enhancing material strength and durability, has been testified even in prehistoric times, as shown by the material characteristics of some plaster floors found in the Pre-Pottery Neolithic site of Asikh Hoyu'k (Anatolia) (Hauptmann and Yalcin, 2000). Microstructural analyses undoubtedly demonstrated the occurrence of mutual interactions between the calcic binders and the numerous micrometric fragments of ignimbritic rocks, showing clear reaction features. It is not clear whether the addition was voluntary or just by chance, considering the high availability of volcanic aggregate in the surrounding area; this constitutes a clear example of the early empirical employment of ad hoc additions in the lime binders to push the microstructural arrangement of the materials toward a better leaching resistance.

Apart from these sporadic findings, a great diffusion of binders composed of lime and various amorphous silicate additions was attested in the buildings of the great Late Bronze Age Mediterranean societies, Minoans and Mycenaeans above all (Shaw, 1973; Chiotis et al., 2001). The technological process of mortar production of the proto-Greek societies entailed the almost systematic addition of finely ground brick powders (*cocciopesto*), whose reactivity in an alkaline environment produced a material with markedly evident waterproofing properties, and thus perfect for lining and plastering purposes (Theodoridou et al., 2013). Such early applications knew diffuse technological transfers in the following centuries along the populations of the Mediterranean basin—Phoenician-Punic, Greeks, and Etruscans—reaching eventually the ancient population that mostly employed such techniques, the Ancient Romans. Starting from the Late Republican Age (Mogetta, 2015), they systematically employed a mix of calcic lime and fine additions mainly constituted of amorphous silicate fractions as binder for their groundbreaking proto-concrete, the *Opus Caementicium*. Such a material constituted from that moment on the structural core of their buildings, no longer consisted of loosely bound shaped stone blocks, but by multileaf rubble masonry, which guaranteed rapid construction times and high durability. The great importance given by Romans to the parametrization of the construction techniques led along the centuries to the writing of several manuals, giving detailed prescriptions on the supply of raw materials, on the mix proportions, and on the casting techniques. Strabo, Seneca, and Pliny the Elder wrote widely in their operas about this new type of binding material, but the most detailed prescriptions can be surely found in the second of the Ten Books on Architecture of Vitruvius, where the author talks about "a kind of powdery earth (*pulvis*) that by its nature produces wonderful results." Vitruvius is referring to the unconsolidated pyroclastites of the Phlegrean Fields near Naples. He specifies that "this material, when mixed with lime and rubble, not only furnishes strength to other buildings,

but also, when breakwaters are built in the sea, they set underwater … and suddenly they are put into contact with water, they cohere into a single mass, quickly solidifying, hardened by the moisture, and neither the effect of the waves nor the effect of water can dissolve them" (Vitruvio, 1997). Such an ancient written source clearly demonstrates the thorough understanding and optimization of the so-called pozzolanic reaction process by the ancient Romans to obtain structural materials characterized by markedly hydraulic properties.

The term "pozzolanic reaction" gathers all the chemical processes occurring among the reactive phases of pozzolana, lime, and water (Massazza, 2002). In more detail, it consists of a recombination of alumino-silicate material and $Ca(OH)_2$ in aqueous solution to form hydrated reaction products (calcium silicate and calcium aluminate hydrates) with binding properties related to their nanostructured crystal habit, according to the following simplified reaction expressed in cement chemistry notation ($A = Al_2O_3$; $C = CaO$; $H = H_2O$; $S = SiO_2$):

$$AS + CH + H \rightarrow C{-}S{-}H + C{-}A{-}H \tag{10.6}$$

On a general basis, any type of alumino-silicate-based material could produce C−S−H and C−A−H phases when blended with lime and water; however, in practice the reaction could occur only if the system is activated or contains already activated phases. The commonly used pozzolanic materials already contain abundant activated phases, namely:

- Glasses in pyroclastic materials
- Zeolitic phases in tuffs
- Amorphous silica in diatomites
- Amorphous phases in burnt clay minerals (*cocciopesto*)

Natural pozzolanic materials of pyroclastic origin were surely supplied according to geographic proximity criteria in prehistoric times, as found in the previously cited mortars from the Asikh Hoyu'k site and in Minoan sites like Akrotiri in Santorini, where abundant pyroclastic materials were already available before the great Thera eruption (Snellings et al., 2012). Such supply criteria were coupled with an early systematic utilization of pozzolanic materials of anthropogenic origin, like *cocciopesto* starting from the Minoan culture and charcoal and ashes of both vegetal and animal origin, first introduced by the Phoenician-Punic civilization (Lancaster, 2012). The employment of these alternative pozzolanic compounds favored a more diffuse application of hydraulic binders, eliminating supply issues related to the sources of natural raw materials. The technology was first transferred to the ancient Greek populations, later reaching the Roman culture, often starting from regions more influenced by the technological exchanges with other Mediterranean cultures like Sardinia (Fig. 10.3A). Furthermore, the Roman technology of pozzolanic binders pushed since the beginning of its development to the systematic

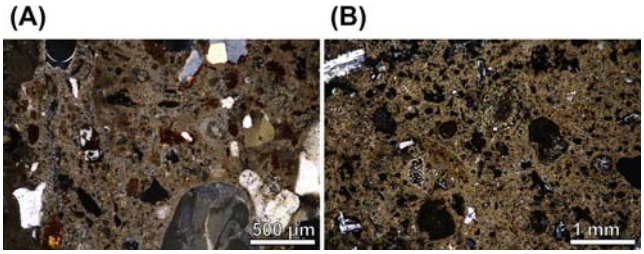

Figure 10.3
Transmitted light optical microscopy images (crossed polars) of Roman pozzolanic binders. (A) Lining mortar of a Roman cistern from the ancient city of Nora, Sardinia (late 3rd century BC), built inside a former Punic tomb: the combined utilization of combustion ashes and *cocciopesto* as pozzolanic additions reflects the technological exchanges between the Roman colony and the Punic populations. (B) *Opus caementicium* from the foundational levels of the Sarno Baths complex in Pompeii (1st century AD): abundant fractions of pumiceous ashes from the Campi Flegrei pyroclastic deposits have been added to confer marked pozzolanic properties to the binders.

quarrying of the most suitable geological sources of pyroclastic materials first individuated in the unconsolidated pumiceous ash levels from Puteoli (the modern Pozzuoli, near Naples) in the Campi Flegrei volcanic district (Fig. 10.3B).

From the Augustan era, after 100 years of experimentation with materials from the Monti Sabatini/Alban Hills volcanic districts, started an almost systematical utilization of the mid-Pleistocene Pozzolane Rosse pyroclastic flow (Jackson et al., 2014; Marra et al., 2016). Such marked standardization led to relevant trades of raw materials throughout all the Roman Empire, from the border regions of the Italian peninsula to the Levant regions, as demonstrated by the finding of Campi Flegrei pozzolanic materials in the structures of the harbor of Caesarea Maritima, Israel (Jackson, 2014). Furthermore, the employment of nonstandardized highly reactive natural pozzolanic materials like diatomaceous earth or natural nanoclays (Fig. 10.4) was still locally adopted in the Roman world previous to the discovery of such big supply sources or during the Late Antiquity, when the collapse of the infrastructural Roman system hindered relevant trades of materials.

It is generally accepted that the pozzolanic reaction process is subdivided into three reaction stages (Snellings et al., 2012), all driven by the difference in Gibbs free energy between reactants and products:

- **Initial dissolution period.** The initial dissolution of $Ca(OH)_2$ produces an alkaline solution saturated in Ca and hydroxyl ions, with a pH over 12. At pH values over 10.7, the solubility of silica and silicates increases continuously (Iler, 1979; Knauss and Wolery, 1988), causing the pozzolana products to dissolve according to processes of hydration, deprotonation, ion adsorption, and hydrolysis at the mineral–water interface, with the

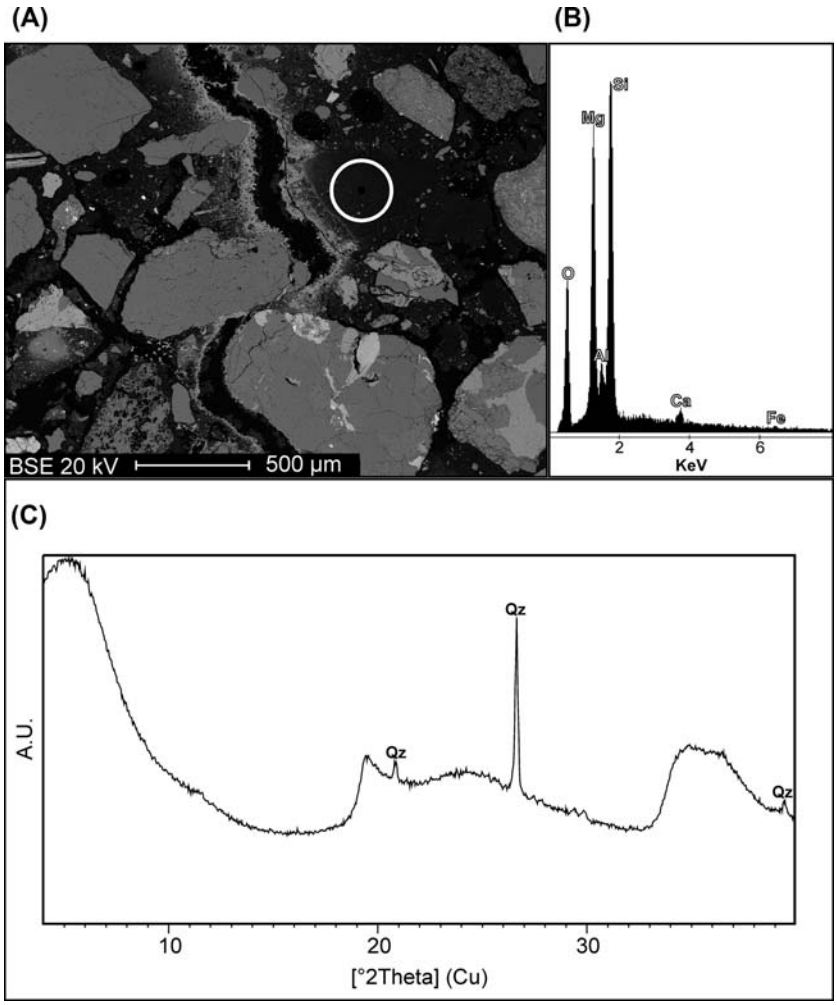

Figure 10.4

(A) SEM-backscattered electron image of *opus caementicium* from the Late Imperial Roman walls of the Torba *castrum* (Castelseprio, North-Western Italy, 5th century AD), employing a paracrystalline and structurally disordered saponite nanoclay as pozzolanic addition, as demonstrated by energy-dispersive microanalyses (B) and X-ray diffraction analyses (C) on clay lumps (traces of nanocrystalline quartz are also present, diffraction peaks indicated with the Qz label).

hydrolysis of the surface silica groups as the rate-controlling step. Dissolution occurs at first in a far-from-equilibrium, highly undersaturated condition, with a progressive slow down of the reaction until reaching $Ca(OH)_2$ saturated conditions. During this phase, a layer of C−S−H phases replaces the external dissolved layers of the pozzolan grains according to topochemical processes, covering the unaltered grain core (Tavasci, 1947), while it is believed the C−A−H phases precipitate far from the pozzolana grains due to

the greater diffusivity of alumina due to the smaller electric charge and lesser oxygen content (Takemoto and Uchikawa, 1980).

- **Induction period.** After the initial dissolution period, a dormant phase occurs, linked to the previously described formation of a protective layer enclosing the reacting pozzolana particles. Such periods terminate after the rupture of the passivating layer, related to its semipermeable characteristics, which allows osmosis of water from the outer to the inner, more concentrated solution, and rupture due to the osmotic pressure (Takemoto and Uchikawa, 1980).
- **Main reaction period.** The rupture of the passivating layer causes a massive triggering of nucleation and growth of reaction products. Such exponential reaction rate increase is short-lived due to the rapid transition toward a diffusion-controlled regime (Držaj et al., 1978; Türker and Yeginobali, 2003; Mertens et al., 2009). Other factors contributing to the slow-down of the reaction are the consumption of the smaller, more reactive, particles and a lack of space or densification of the C−S−H rim that hinders the free growth of the hydrate particles (Snellings et al., 2012). From this moment on, the reaction process proceeds indefinitely until total drying of the system or total consumption of the reactants.

Despite the numerous types of pozzolanic materials available, the final reaction products are rather similar, and the phase assemblages present strong similarities with the ones typical for Portland cement. This is due to an overall affinity in the chemical composition of the reactive fractions, resulting in few phases being thermodynamically stable at ambient conditions (Snellings et al., 2012). The silicate fraction released from the pozzolan combines with the calcium ions to form C−S−H, a wide family of minerals of the tobermorite group with variable Ca/Si ratios, depending on the activity and composition of the pozzolan and on the mix design (Richardson, 2008). Upon time, an increase in polymerization of the silicate groups can be observed (Massazza and Testolin, 1983; Brough et al., 1995).

Dissolved alumina either incorporates within the C−S−H phases, producing compounds defined as C−A−S−H (Richardson et al., 1993), or combines directly with calcium ions to form calcium aluminate hydrates, also defined as AFm phases (Matschei et al., 2007). In absence of sulfate, carbonate, or chloride ions, the thermodynamically favored AFm phases are C_4AH_{13-19} (Taylor, 1997), but the occurrence of strätlingite (hydrated ghelenite), C_2ASH_8 can also be observed after the recombination of alumina and silica with calcium ions in the presence of general or local deficiencies of $Ca(OH)_2$ (Serry et al., 1984; Ambroise et al., 1994). Furthermore, katoite (hydrogarnet C_3AH_6) could be stabilized during later reaction stages, when combined lime represents 40%−60% of the initial pozzolana mass, in the presence of high water/solid ratios and abundant alkalis (Takemoto and Uchikawa, 1980).

When soluble sulfate are present, the precipitation of ettringite $C_6A\overline{S}_3H_{32}$, monosulfoaluminate (kuzelite $C_4A\overline{S}H_{12}$), or a combination of both depending on the sulfate-to-alumina ratio, could occur (Taylor, 1997). Furthermore, upon air exposure or in the presence of abundant carbonate in the mortar either due to precipitation of anthropogenic calcite from lime carbonation or due to the presence of carbonate aggregates, C_4AH_{13} undergoes carbonation processes, transforming into hemicarboaluminate $C_4A\overline{C}_{0.5}H_{12}$ and/or monocarboaluminate $C_4A\overline{C}H_{11}$ (Matschei et al., 2007). Finally, in diagenized high silica materials with low percentages of other oxides like diatomaceous earths, only C−S−H precipitates (Takemoto and Uchikawa, 1980).

Microstructural analyses on Roman pozzolanic mortars always show relevant dissolution features on the relicts of pozzolanic material (Fig. 10.5A) with increasing Ca/Si ratios toward the interface with the surrounding matrix (Fig. 10.5B and C), indicating the interfacial nature of the pozzolanic reaction. The binding matrices (Fig. 10.5D) are

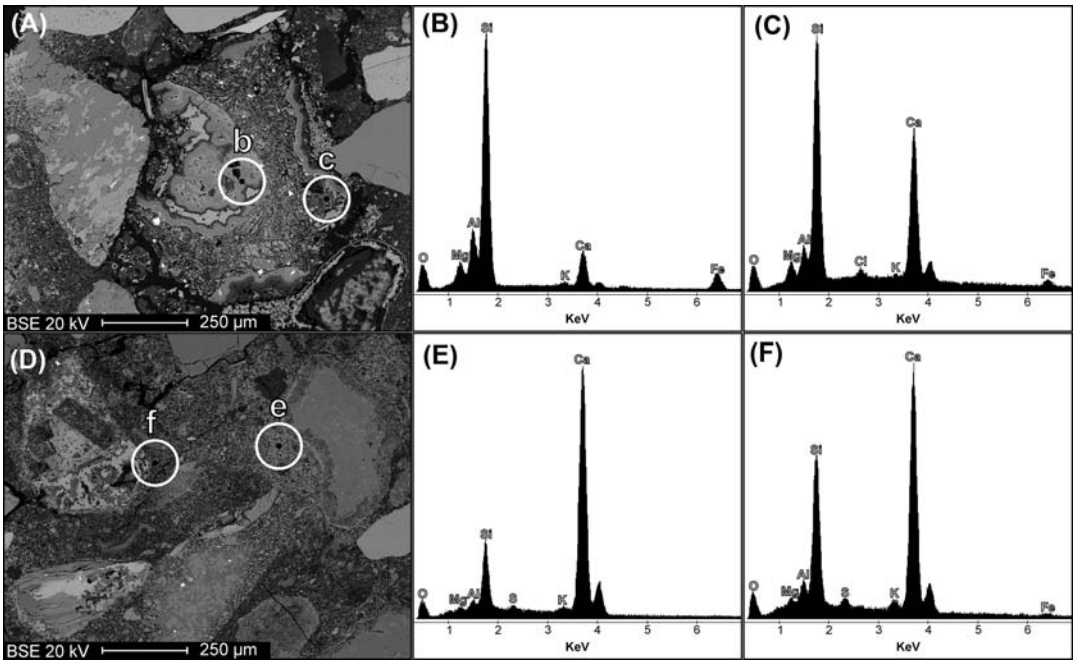

Figure 10.5

SEM-EDS analyses on *opus caementicium* samples from the Roman amphitheater of Padova (Northeastern Italy, 1st century AD), employing imported volcanic materials from the Pozzolane Rosse pyroclastic flow as reactive aggregate, together with local carbonate sand. (A) Back-scattered electron image (BEI) of a pyroclastic aggregate with marked dissolution features due to the pozzolanic reaction and EDS analyses of its core (B) and rims (C). (D) BEI of the binder matrix and EDS analyses of the reacted binder close to a carbonate (E) and pyroclastic (F) aggregate.

univocally composed of dense clusters of unresolved nanocrystals mainly composed of Ca, Si, and Al with variable relative ratios, often strongly influenced by the local occurrence of reactive pozzolanic particles. On a general basis, increasing Ca/Si ratios are observable in the portions distant from the reactive grains (Fig. 10.5E and F), suggesting the occurrence of mixes of pozzolanic C−S−H, C−A−S−H and C−A−H phases and anthropogenic calcium carbonates due to partial aerial reaction of lime.

Mineralogical analyses by standard XRPD on the binding matrices (Fig. 10.6) clearly confirm the paracrystalline and nanophasic nature of the hydrated phases: the occurrence of C−A−H phases is generally attested by the presence of AFm basal peaks with high full width at half maximum (FWHM) values and computed mean crystallite sizes always lower than 30 nm. As for the silicate component, C−S−H and C−A−S−H phases are frequently recognizable only through a diffuse scattering at lower angular values, sometimes coupled with broad basal diffraction peaks related to the [020] crystallographic direction. The occurrence of more crystalline C−S−H and C−A−S−H phases, with several recognizable

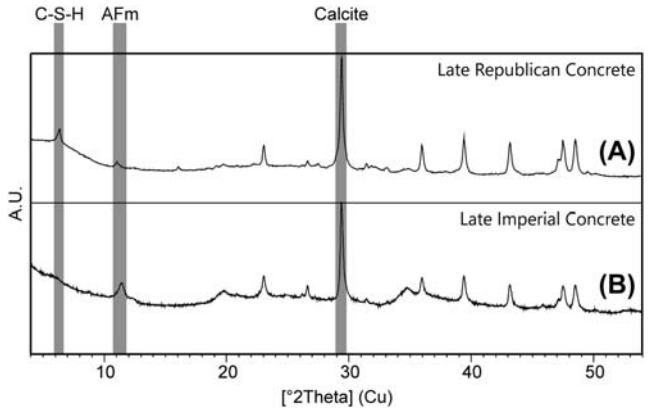

Figure 10.6

X-ray diffraction patterns of the binder fractions of two different Roman concretes, with the main diffraction peaks of the reaction phases indicated. (A) Late Republican concrete from the foundational levels of the city walls of Aquileia (Northeastern Italy, beginning of the 2nd century BC): the utilization of highly siliceous pumiceous ashes as aggregate allowed a relevant crystallization of C−S−H phases, with recognizable diffraction peaks indicating the occurrence of a crystalline tobermorite fraction, associated with a more disordered fraction contributing to the increase of the low angle scattering. (B) Late Imperial concrete from the walls of the Torba *castrum* (Castelseprio, Northwestern Italy, 5th century AD): the utilization of Mg and Al rich saponite nanoclays as aggregate favored the abundant crystallization of low-crystallinity AFm phases, as indicated by the high full width at half maximum of basal peaks, while the occurrence of a disordered C−S−H fraction is recognizable through the diffuse low-angle scattering. Calcite is present in both samples, indicating partial aerial reaction of the lime.

diffraction peaks apart from the basal one, is observable only for concrete prepared with extremely reactive pozzolanic additions like finely ground pumiceous ashes.

Advanced mineralogical studies on ancient Roman concretes, combining synchrotron-based XRD and micro-XRD and ^{29}Si and ^{27}Al nuclear magnetic resonance (NMR) (Jackson et al., 2013, 2014), indicated that the pozzolanic matrices in the relict lime clasts are composed of Al-tobermorite, with Al^{3+} substitution for Si^{4+} in $Q^2(1Al)$, $Q^3(1Al)$, and $Q^3(2Al)$ tetrahedral chain and branching sites. Furthermore, a poorly crystalline C−A−S−H binder crystallized in the dissolved perimeter of the relict lime clasts, with $Ca/(Si + Al) = 0.79$ affine to the one of Al-tobermorite but characterized by the occurrence of nanoscale heterogeneities with aluminum in both tetrahedral and octahedral coordination. Finally, the occurrence of dense clusters of fibrous strätlingite crystals has been observed in the interfacial transition zones between the cementing paste and the scoria aggregates (Fig. 10.7). The experimental reproduction of a Roman concrete (Jackson et al., 2014) allowed to observe the evolution of its cementitious matrix upon aging: at 28 days, it is composed of irregular patches of C−A−S−H with variable composition and associated C−A−H fibrous crystals. At later reaction stages (90 and 180 days), when portlandite is entirely consumed, a marked growth and coalescence of the C−A−S−H clusters is observable, enriched in aluminum and alkalis. The occurrence of alkalis is a mitigating factor for alkali-silica reaction, even after repeated saturation with floodwaters. Interfacial strätlingite formation is also observable in later reaction stages. Fibrous strätlingite crystals in Imperial Roman mortars are affine to the microfibers commonly added to modern cement pastes to increase tensile strength, but their natural in situ crystallization in the interfacial transition zones, notoriously recognized as the

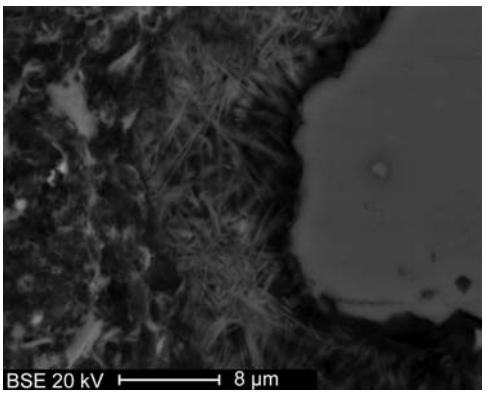

Figure 10.7

Late Republican concrete from the foundational levels of the city walls of Aquileia (Northeastern Italy, beginning of the 2nd century BC), backscattered electron image of the interfacial transition zone between binding matrix and an aggregate particle, showing the occurrence of dense clusters of fibrous silico-aluminate crystals formed after pozzolanic reaction processes.

weakest concrete portions (Scrivener et al., 2004), is surely a crucial factor in enhancing mechanical strength in Roman hydraulic binders.

Such beneficial effects are not observable through classic uniaxial compressive and tensile strength tests, generally giving results between 1/5 and 1/10 of modern structural concretes (Jackson et al., 2009, 2014; Jackson, 2014). On the other hand, they are clearly evident in the fracture energy values; that is, the amount of mechanical work required to propagate a macrocrack of one square unit of new surface area (Hillerborg, 1985), generally attested close to one-half with respect to modern concrete. Another factor contributing to the excellent mechanical and durability properties of Roman pozzolanic binders is the low amount of capillary microporosity with respect to modern cementitious binders, due to the slow reaction kinetics that produce limited temperature rise during exothermic reaction processes (Brune, 2011). Finally, they are characterized by self-healing properties due to continuous precipitation phenomena of hydrated compounds after delayed dissolution of the pozzolanic matrices in presence of moisture permeating the concrete fabric (Jackson, 2014).

Analytical studies on ancient pozzolanic binders clearly confirmed the fundamental role of this technological evolution to tailor the nanoscale structural properties of the materials, enhancing both macroscale mechanical properties and durability and being at the same time a relevant source of inspiration for the formulation of modern-low environmental impact structural binders.

10.4 Modern Binders: Portland Cement

The modern construction industry has been dominated, for nearly two centuries, by Portland cement, which was patented by Joseph Aspdin in 1824. Aspdin obtained this material by crushing limestone, mixing it with clay and calcining the mixture. Since then, the properties of Portland cement have been progressively optimized, but the basic recipe still remains that of Aspdin and currently, over 4 billion tons of cement are produced each year (Fig. 10.8).

The systematic scientific study of cement began at the end of the 19th century. The use of optical microscopy led to the definition of four different phases as the constituents of Portland cement (Blezard, 1998). These phases consist of calcium silicates and calcium aluminates formed upon heating of the raw mix to 1450°C and subsequent cooling (Table 10.1). The reaction of these phases with water and a small quantity of gypsum (added, normally up to 5 wt%, as a set regulator) consists of a set of complex dissolution-precipitation reactions. Immediately after contact with the mix water the four cement phases and gypsum begin to dissolve, each with a different rate, releasing ionic species in the aqueous solution that, upon reaching saturation with respect to hydrated phases, form

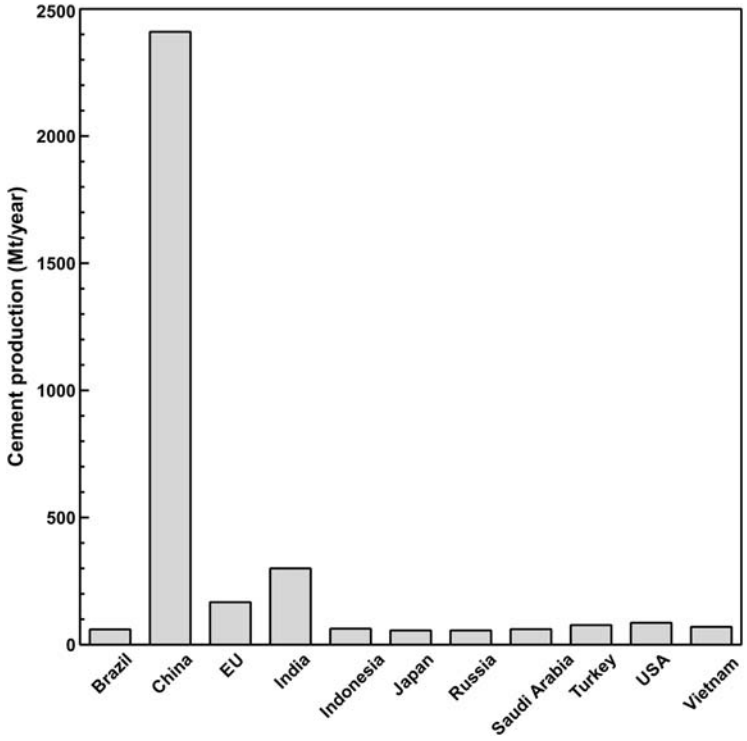

Figure 10.8
Main worldwide cement producers. *Data from U.S. Geological Survey, 2017. Mineral Commodity Summaries.*

Table 10.1: Summary of the phases present in Portland cement.

Phase	Composition	Notation
Alite	Ca_3SiO_5	C_3S
Belite	Ca_2SiO_4	C_2S
Aluminate	$Ca_3Al_2O_6$	C_3A
Ferrite	$Ca_4Al_2Fe_2O_{10}$	C_4AF

Cement Chemistry Notation: *A*, Al_2O_3; *C*, CaO; *F*, Fe_2O_3; *S*, SiO_2.

reaction products. This process leads, from a macroscopic viewpoint, to the formation of a viscous slurry that eventually sets and evolves to an elastic solid.

The main hydration product of Portland cement is a calcium-silicate hydrate, commonly referred to as C−S−H using cement chemistry notation. C−S−H is characterized by a pseudotobermoritic defective crystal structure that forms nanoscale aggregates and conveys cohesive properties to hydrated cement (Taylor, 1986; Kirkpatrick et al., 1997; Skinner et al., 2010; Kovačević et al., 2015). C−S−H precipitation consists of a first nucleation

step, during which new interfaces are formed in the aqueous solution (homogeneous nucleation) or at preexisting interfaces (heterogeneous nucleation). Nucleation is followed by growth or aggregation of nuclei, as more ionic species are withdrawn from solution and attached to new C−S−H surfaces. This process leads to the formation of a nanostructured, X-ray amorphous matrix.

In recent years, the properties resulting from the nanostructure of C−S−H have been exploited to manufacture specific additives consisting of nanocomposites formed by synthetic C−S−H aggregates precipitated in the presence of stabilizing polymers (Fig. 10.9). Such additives have been used mostly as accelerating admixtures, with the aim of increasing the rate of cement hydration and the subsequent development of mechanical properties (Alizadeh et al., 2009; Nicoleau, 2013; Sun et al., 2017). The accelerating effect is related to the seeding effect of the C−S−H nanocomposites, whose large specific surface area provides sites for the attachment of particles contributing to C−S−H growth during the early stages of cement hydration (Thomas et al., 2009; Artioli et al., 2014).

More recently, such nanocomposites also found applications as permeability reducing agents (Ferrari et al., 2007).

Classical and current views on C−S−H nanostructure and precipitation mechanisms, as well as C−S−H interaction with organic molecules, are discussed in the following section.

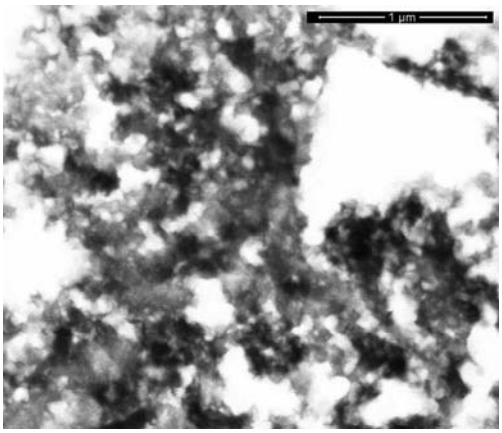

Figure 10.9
STEM image of C−S−H nanocomposite aggregate.

10.5 Mechanisms of Calcium-Silicate Hydrate Nanostructure Formation

10.5.1 Classical Models of C–S–H Nanostructure

The advent of X-ray crystallography in the 20th century gave momentum to the development of the first structural models of C–S–H, which postulated the existence of a layered structure (Bernal et al., 1952). Elaborating on the evidence of a layered structure, Feldman and Sereda (1970) developed a model that described the C–S–H nanostructure as a continuous and disordered assemblage of layers in which H_2O molecules are either adsorbed to the surface or entrapped in the space between such buckled layers (Fig. 10.10A). This model provided insight into C–S–H structure and provided some

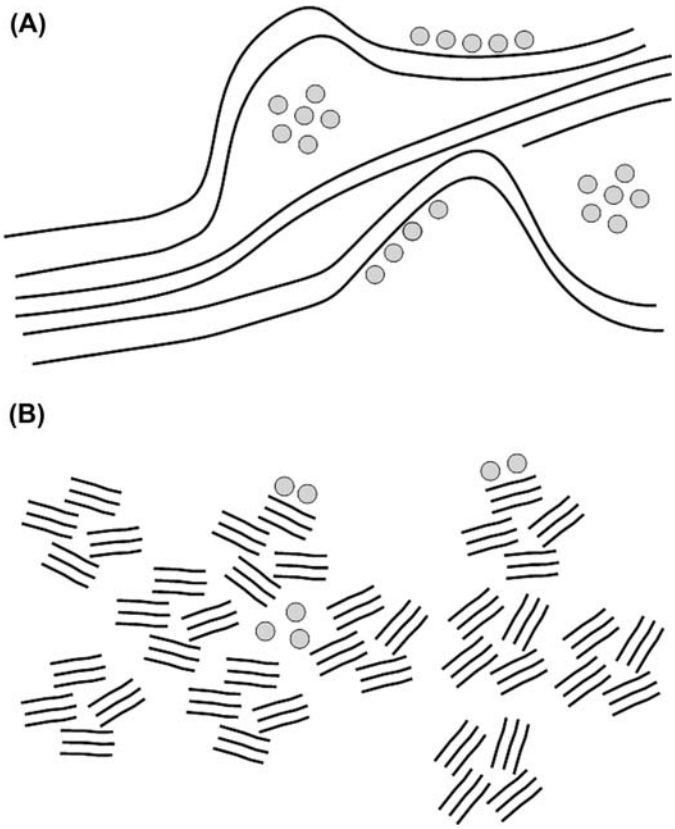

Figure 10.10

Sketch of the Feldman-Sereda (A) and colloidal (B) models. The *filled circles* represent H_2O molecules (not to scale) adsorbed to surfaces or entrapped in the nanopores. *Redrawn based on Feldman, R.F., Sereda, P.J., 1970. New model for hydrated Portland cement and its practical implications. Engineering Journal 53, 53–59; Jennings, H.M., 2008. Refinements to colloid model of C-S-H in cement: CM-II. Cement and Concrete Research 38, 275–289.*

support for measurable quantities as specific surface area. Although highly simplified, it is still currently advocated as a possible realistic view of the C−S−H nanostructure.

The other dominant model, often referred to as colloidal model, envisages a C−S−H nanostructure consisting of a hierarchical aggregation of layered building blocks (Fig. 10.10B), each having a size of approximately 4 nm (Jennings, 2004, 2008). This model has been corroborated by small angle neutron scattering data that suggested the existence of a hierarchical structure of layered, nanosized particles, which could be described by a fractal dimension (Allen et al., 1987; Chiang et al., 2012). Direct observation of the aggregation of such particles over preexisting substrates could be achieved by means of atomic force microscopy (Nonat, 2004; Garrault et al., 2005).

More comprehensive reviews of early models of C−S−H nanostructure and their evolutions can be found in (Richardson, 2008; Papatzani et al., 2015).

Though these nanostructural models can provide explanations for some experimentally observed properties, they are still somewhat simplified and difficult to reconcile with the modern views on phase separation and the processes of nucleation, growth, and aggregation in aqueous solution. The next sections will give an overview of how the development of C−S−H nanostructure could be linked with such basic processes by combining different computational and experimental approaches.

10.5.2 C−S−H Characterization by X-Ray Scattering-Based Techniques

Consistent with its nanostructured nature, XRD diffraction patterns of C−S−H display the characteristics of semiamorphous materials, with only few and broad diffraction peaks (Fig. 10.6). In particular, C−S−H diffraction patterns resemble those obtained from the variety of the mineral group tobermorite having a basal spacing of 14 Å, with crystallite size of the order of 10 nm and turbostratic disorder (Grangeon et al., 2013). Tobermorite 14 Å is characterized by a stacked layered structure consisting of a central sheet with Ca coordinated by seven O atoms, connected to chains of Si having a periodicity of three tetrahedral, with Ca and H_2O in the interlayer (Bonaccorsi et al., 2005). However, tobermorite is characterized by a Ca/Si ratio of 0.8, whereas the Ca/Si of C−S−H precipitating in hydrating Portland cement has a value of 1.7 in mature pastes (Taylor, 1997). Different hypotheses were proposed to explain the observed discrepancy in Ca/Si ratio, including the possibility for C−S−H to precipitate as a mixture of tobermorite and jennite (a calcium silicate hydrate with Ca/Si = 1.5) (Taylor, 1986). This hypothesis has progressively lost consensus in favor of other models that envisage a random removal of Si tetrahedral from the infinite chain of tobermorite, replacement of protons with Ca in the interlayer, and insertion of additional Ca in the interlayer, charge balanced by hydroxyl ions (Kovačević et al., 2015).

In order to overcome the intrinsic limitations of implementing XRD for the study of the defective nanocrystalline structure of C−S−H, recent successful attempts have been carried out to assess the local, short-range order by synchrotron radiation pair distribution function analysis (Skinner, 2010; Soyer-Uzun et al., 2012; Cuesta et al., 2017; Grangeon et al., 2017). These studies confirmed the nanocrystalline nature of C−S−H and the existence of structured domains of a few nanometers.

10.5.3 Numerical Simulations of C−S−H Aggregation Dynamics

Currently accepted models of C−S−H local ordering and nanostructural arrangement do not shed light on the basic mechanisms leading to the formation of such nanostructured aggregates. Several numerical models have been devised with the aim of simulating the formation of nanoparticle aggregates, using molecular dynamics and Monte Carlo approaches (Dolado et al., 2011; Masoero et al., 2012; Gonzalez-Teresa et al., 2013; Ioannidou et al., 2016; Shvab et al., 2017). These simulations generally produce domains of tens to a few hundred nanometers consisting of aggregation of hard spheres and reproduce, with good accuracy, experimentally observable properties such as rate of hydration, nanopore size distribution, scattering intensity and indentation moduli.
The main limitation of such colloidal models stems from the lack of knowledge about the modes of formation of the particles present in the simulation domain. For example, the aggregation of such particles throughout the available volume is not easy to reconcile with the experimental observation that, in normal hydration conditions, the formation of C−S−H nuclei occurs in close proximity of preexisting surfaces, resembling a process of heterogeneous nucleation (Garrault-Gaffinet and Nonat, 1999; Valentini et al., 2012).
One step forward in this direction was taken by recent research based on Monte Carlo simulations of the aggregation of C−S−H platelets (Delhorme et al., 2016). The results of these simulations showed that the formation of stacked C−S−H aggregates on charged C_3S surfaces is energetically favored at high Ca concentration in solution. Moreover, it was shown that in the absence of charged surfaces, the tendency of two platelets to attract each other is much smaller. Based on previous Monte Carlo simulations, showing that the growth of C−S−H platelet is hindered by slow kinetics (Labbez et al., 2014), the authors of this study suggest that C−S−H precipitation proceeds by an autocatalytic process by which the presence of C−S−H platelets adsorbed onto C_3S surfaces stimulates the formation of new C−S−H nuclei. Although these studies contributed significantly to the advance in the understanding of the possible mechanisms of C−S−H aggregation during cement hydration, there are still many open questions about how C−S−H nucleation is initiated and what the pathways leading to the formation of such nanosized platelets are.

10.5.4 Interaction Between C–S–H and Organic Molecules

The control of cement properties by means of organic molecules was already practiced by the Romans, who added egg white or animal blood to concrete (Aïtcin, 2008). Nowadays, organic additives represent a fundamental ingredient for the production of concrete with enhanced properties (Aïtcin and Flatt, 2016).

Organic molecules have a strong tendency to interact with inorganic phases and alter the pathways to the formation of new precipitates. By adsorbing onto inorganic surface, they can interfere with the process of nucleation and growth and modify the crystalline habit of minerals (Rodriguez-Navarro and Benning, 2013). Polycarboxylate ether (PCE) superplasticizers, a class of cement admixtures based on polycarboxilate comb polymers, used to control cement rheology, make no exception to this general behavior. PCEs are among the most widely used cement admixtures and they have been shown to interact with inorganic phases such as calcite, by acting as templates for calcite precipitation, inducing significant changes in crystalline habit (Keller and Plank, 2013).

PCE admixtures also strongly affect the kinetics of cement hydration, in particular by significantly reducing the rate of reaction. The inhibition of cement hydration is believed to result from the interaction of PCE molecules with both anhydrous phases (Suraneni and Flatt, 2015; Marchon et al., 2017) and hydration products (Mollah et al., 2000). Inhibition of the rate of C–S–H nucleation in the presence of PCE is predicted by kinetic modeling (Valentini et al., 2016). This model also predicted a switch from heterogeneous to homogeneous C–S–H nucleation, induced by the interaction with PCE molecules. Loss of correlation with preexisting surfaces, when superplasticizers are added to the system, were also supported by experimental imaging methods based on synchrotron XRD-tomography (Artioli et al., 2015). Measurements performed by ultracentrifugation confirmed this hypothesis and suggested that, in the presence of PCE, C–S–H nucleation may be initiated by Ca complexation by the negatively charged backbone of PCE comb polymers, leading to the formation of prenucleation clusters, followed by the aggregation of such entities to form stable C–S–H particles precipitating away from preexisting surfaces (Sowoidnich et al., 2015).

10.5.5 Toward a Refined Model of Nanostructural Development

The combination of advanced experimental and numerical methods allowed the definition of more realistic views of C–S–H nanostructural development, starting from the early layered and colloidal models. The design of modern cement binders and nanocomposite admixtures would benefit from a knowledge-based approach that requires further research to unravel the dynamics of C–S–H nanostructure formation and reconcile it with the current views on nucleation and growth.

The classical theory of nucleation and growth has been revised and the role of nonclassical pathways to phase separation is receiving more and more attention (van Driessche et al., 2017). These theories challenge the classical view of nucleation and growth as a process of monomer by monomer attachment to metastable nuclei or stable surfaces and envisage the formation of a variety of intermediate precursor to the final bulk phase, ranging from ionic clusters to amorphous nanoparticles (De Yoreo et al., 2015).

As anticipated in the previous section, one intriguing possibility is the formation of prenucleation clusters as precursors of C−S−H nanoparticles that eventually evolve to a fractal aggregate. Prenucleation clusters are defined as thermodynamically stables particles, having size of a few nm, formed by the association of solute entities and represent solute precursors to the formation of new phases (Gebauer, 2016).

Such clusters may form by complexation of Ca cation and Si counterions in PCE additivated cement (Fig. 10.11) and may constitute solute precursors to the formation of C−S−H nanosized aggregates. Specifically designed experiments, for example by synchrotron small-angle X-ray scattering, will be needed in order to shed light on the earliest stage of C−S−H nucleation and confirm the hypothesized formation of PCE/C−S−H prenucleation clusters.

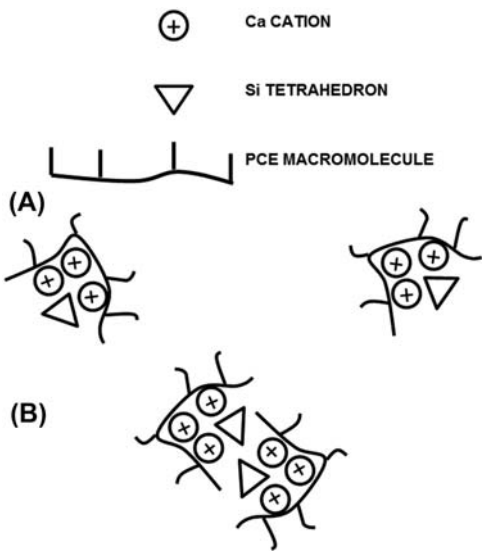

Figure 10.11
Sketch of the possible mechanisms leading to the formation of PCE/C−S−H clusters. (A) Complexation of Ca cations and Si counterions. (B) Cluster aggregation.

10.6 Beyond Portland Cement: Nanostructured Binders for a Sustainable Future

Cement binders represent an essential material for the built environment. Their robustness and reliability are testified by the fact that the basic raw materials and formulations have not changed much since the rise of the Roman empire, two millennia ago. Nonetheless, society and the scientific community are now facing the issue of replacing Portland cement with equally well-performing, but more sustainable binders. Although the footprint per unit mass of Portland cement is low compared to other manufactured materials, its huge annual production currently contributes to more than 5% of the total anthropogenic CO_2 emitted (Barcelo et al., 2014). The main source of CO_2 emissions are associated with the calcination of limestone, which represents about 85% of the raw materials employed for Portland cement production. One possible solution to this issue is reducing the output of Portland cement produced by encouraging the use of blends in which a fraction of Portland cement is substituted by other materials having pozzolanic properties, including calcined clays and industrial by-products (such as fly ash from coal combustion, or ground granulated blast-furnace slag from the steel industry). Depending on the type of material used in the blends, modifications in the structure and chemical composition occur in the C−S−H hydration product, which retains its nanocrystalline nature (Manzano et al., 2009; Pegado et al., 2014). As an alternative to blended cements, Portland-free binders may be obtained by chemical activation of the materials used in the aforementioned blends (i.e., calcined clays, fly ash, slag, as well as agricultural waste such as rice husk ash) using alkaline solutions (mostly sodium hydroxide and sodium silicate solutions) (Provis and van Deventer, 2014). The reaction products of alkali-activated cements consist of gels having the same X-ray amorphous nature in common with C−S−H. The exact nature and structure of these gels is still debated, although the possibility for this product to consist of nanocrystalline domains has been suggested (Provis et al., 2005).

Currently, much effort is being dedicated to testing the performance and durability of such alternative binders in practical applications. Parallel to such an applied approach, more basic research aimed at clarifying the processes associated with the formation of the reaction products of alternative binders would be beneficial in order to implement a knowledge-based approach to the development of novel binders, characterized by a significantly reduced environmental footprint.

References

Aïtcin, P.C., Flatt, R.J., 2016. Science and Technology of Concrete Admixtures. Woodhead Publishing, Sawston, UK.

Aïtcin, P.C., 2008. Binders for Durable and Sustainable Concrete. Taylor & Francis, London, UK.

Alizadeh, R., Raki, L., Makar, J.M., Beaudoin, J.J., Moudrakovski, I., 2009. Hydration of tricalcium silicate in the presence of synthetic calcium−silicate−hydrate. Journal of Materials Chemistry 42, 7937−7946.

Allen, A.J., Oberthur, R.C., Pearson, D., Schofield, P., Wilding, C.R., 1987. Development of the fine porosity and gel structure of hydrating cement systems. Philosophical Magazine B 56, 263−288.

Ambroise, J., Maximilien, S., Péra, J., 1994. Properties of metakaolin blended cements. Advanced Cement Based Materials 1, 161−168.

Artioli, G., Valentini, L., Dalconi, M.C., Parisatto, M., Voltolini, M., Russo, V., Ferrari, G., 2014. Imaging of nano-seeded nucleation in cement pastes by X-ray diffraction tomography. International Journal of Materials Research 105, 628−631.

Artioli, G., Valentini, L., Voltolini, M., Dalconi, M.C., Ferrari, G., Russo, V., 2015. Direct imaging of nucleation mechanisms by synchrotron diffraction micro-tomography: superplasticizer-induced change of C−S−H nucleation in cement. Crystal Growth and Design 15, 20−23.

Aspdin, J., 1824. Producing an Artificial Stone. British Patent BP 5022.

Barbisan, U., Guardini, M., 2007. Reinforced Concrete: A Short History. Tecnologos, Mantova, IT.

Barcelo, L., Kline, J., Walenta, G., Gartner, E., 2014. Cement and carbon emissions. Materials and Structures 47, 1055−1065.

Bar-Yosef, O., Goring-Morris, A.N., 1977. Geometric Kebaran occurrences. In: Bar-Yosef, O., Phillips, J.L. (Eds.), Prehistoric Investigations in Gebel Magh- ara, Northern Sinai, Qedem 7. Monographs of the Institute of Archaeology. The Hebrew University, Jerusalem, IL, pp. 331−368.

Bar-Yosef, O., 1983. The natufian in the Southern levant. In: Cuyler Young, T., Smith, P.E.L., Mortensen, P. (Eds.), The Hilly Flanks and beyond. Studies in Ancient Oriental Civilizations 36. University of Chicago Oriental Institute, Chicago, USA, pp. 11−42.

Bensted, J., Coleman, N.J., 2004. La sorprendente storia del cemento e del calcestruzzo dalle origini dell'Età della Pietra al 1900 d.C. L'Industria Italiana del Cemento 801, 692−771.

Bensted, J., 1997. Inaugural Lectures Series, University of Greenwich. Cement: Past, Present and Future. Dartford Greenwich University Press, Greenwich, UK.

Bernal, J.D., Jeffery, J.W., Taylor, H.F.W., 1952. Crystallographic research on the hydration of Portland cement. A first report on investigations in progress. Magazine of Concrete Research 4, 49−54.

Blezard, R.G., 1998. The history of calcareous cements. In: Hewlett, P.C. (Ed.), Lea's Chemistry of Cement and Concrete. Elsevier, Oxford, UK, pp. 1−24.

Bohac, M., Necas, R., 2016. The role of aging on rheological properties of lime putty. Procedia Engineering 151, 34−41.

Bonaccorsi, E., Merlino, S., Kampf, A.R., 2005. The crystal structure of tobermorite 14 Å (plombierite), a C−S−H phase. Journal of the American Ceramic Society 8, 505−512.

Brough, A.R., Dobson, C.M., Richardson, I.G., Groves, G.W., 1995. A study of the pozzolanic reaction by solid-state 29^{Si} nuclear magnetic resonance using selective isotopic enrichment. Journal of Materials Science 30, 1671−1678.

Brune, P., 2011. The Mechanics of Imperial Roman Concrete and the Structural Design of the Vaulted Monuments (Ph.D. dissertation). Univ of Rochester, Rochester, NY.

Cagnana, A., 2000. I leganti, gli intonaci, gli stucchi in archeologia dei materiali da costruzione. In: Crogiolo, G.P., Olcese, G. (Eds.), Manuali per'archeologia, pp. 123−154. Como, IT, Ed. S.A.P. s.r.l.

Catone, M.P., 2000. De Agricoltura. Mondadori, Milano, IT.

Cazalla, O., Rodriguez-Navarro, C., Sebastian, E., Cultrone, G., de la Torre, M.J., 2000. Ageing of lime putty: effects on traditional lime mortar carbonation. Journal of the American Ceramic Society 83 (5), 1071−1076.

Chiang, W.S., Fratini, E., Baglioni, P., Liu, D., Chen, S.H., 2012. Microstructure determination of calcium-silicate-hydrate globules by small-angle neutron scattering. Journal of Physical Chemistry C 116, 5055−5061.

Chiotis, E., Dimou, E., Papadimitriou, G.D., Tzoutzopoulos, S., 2001. The study of some ancient and prehistoric plasters and watertight coatings from Greece. In: Aloupi, E., Bassiakos, Y., Facorellis, Y.

(Eds.), Archaeometry Issues in Greek Prehistory and Antiquity. Hellenic Society for Archaeometry and the Society of Messenean Archaeological Studies, Athens, GR, pp. 327–342.

Cizer, O., 2016. Lime mortars in heritage: fundamental insights into carbonation reaction and its biocatalization. In: Van Balen, K., Verstrynge, E. (Eds.), Structural Analysis of Historical Constructions: Anamnesis, Diagnosis, Therapy, Controls. Taylor and Francis Group, London, UK, pp. 67–74.

Cizer, Ö., Van Balen, K., Elsen, J., 2012. Real-time investigation of reaction rate and mineral phase modifications of lime carbonation. Construction and Building Materials 35, 741–751.

Collepardi, M., 2003. La lezione dei Romani: durabilità e sostenibilità delle opere architettoniche e strutturali. In: Proceedings of the III Convegno AIMAT "Restauro e conservazione dei beni culturali: materiali e tecniche". Cassino, IT.

Cuesta, A., Zea-Garcia, J.D., Londono-Zuluaga, D., De la Torre, A.G., Santacruz, I., Vallcorba, O., Aranda, M.A.G., 2017. Synchrotron radiation pair distribution function analysis of gels in cements. Crystals 7, 317.

De Yoreo, J.J., Gilbert, P.U.P.A., Sommerdijk, N.A.J.M., Penn, R.L., Whitelam, S., Joester, D., Zhang, H., Rimer, J.D., Navrotsky, A., Banfield, J.M., Wallace, A.F., Michel, F.M., Meldrum, F.C., Cölfen, F.C., Dove, P.M., 2015. Crystallization by particle attachment in synthetic, biogenic, and geologic environments. Science 349 aaa6760.

Delhorme, M., Labbez, C., Turesson, M., Lesniewska, E., Woodward, C.E., Jönsson, B., 2016. Aggregation of calcium silicate hydrate nanoplatelets. Langmuir 32, 2058–2066.

Dolado, J.S., Griebel, M., Hamaekers, J., Heber, F., 2011. The nano-branched structure of cementitious calcium-silicate-hydrate gel. Journal of Materials Chemistry 21, 4445–4449.

Držaj, B., Hočevar, S., Slokan, M., Zajc, A., 1978. Kinetics and mechanism of reaction in the zeolitic tuff-CaO-H2O systems at increased temperature. Cement and Concrete Research 8, 711–720.

Feldman, R.F., Sereda, P.J., 1970. New model for hydrated Portland cement and its practical implications. Engineering Journal 53, 53–59.

Ferrari, G., Russo, V., Salvioni, D., Surico, F., Artioli, G., Dalconi, M.C., Secco, M., Valentini, L., 2007. The influence of a new metal silicate hy drate admixture on concrete strength and durability. ACI Special Publications 29926, 83–92.

Garrault, S., Finot, S., Lesniewska, E., Nonat, A., 2005. Study of C–S–H growth of C_3S surface during its early hydration. Materials and Structures 38, 435–442.

Garrault-Gauffinet, S., Nonat, A., 1999. Experimental investigation of calcium silicate hydrate (C–S–H) nucleation. Journal of Crystal Growth 200, 565–574.

Gebauer, D., 2016. Prenucleation clusters. In: Bhushan, B. (Ed.), Encyclopedia of Nanotechnology. Dordrecht, the Netherlands. Springer.

Gonzalez-Teresa, R., Dolado, J.S., Ayuela, A., Gimel, J.C., 2013. Nanoscale texture development of C–S–H gel: a computational model for nucleation and growth. Applied Physics Letters 103, 234105.

Grangeon, S., Claret, F., Linard, Y., Chiaberge, C., 2013. X-ray diffraction: a powerful tool to probe and understand the structure of nanocrystalline calcium silicate hydrates. Acta Crystallographica Section B 69, 465–473.

Grangeon, S., Fernandez-Martinez, A., Baronnet, A., Marty, N., Poulain, A., Elkaïm, E., Roosz, C., Gaboreau, S., Henocq, P., Claret, F., 2017. Quantitative X-ray pair distribution function analysis of nanocrystalline calcium silicate hydrates: a contribution to the understanding of cement chemistry. Journal of Applied Crystallography 50, 14–21.

Hansen, E., Rodríguez-Navarro, C., Van Balen, K., 2008. Lime putties and mortars, insights into fundamental properties. Studies in Conservation 53 (1), 9–23.

Hauptmann, A., Yalcin, Ü., 2000. Lime plaster, cement and the first puzzolanic reaction. Paleorient 26 (2), 61–68.

Hillerborg, A., 1985. Results of three comparative test series for determining the fracture energy gf of concrete. Materials and Structures 18, 407–413.

Iler, R.K., 1979. The Chemistry of Silica: Solubility, Polymerization, Colloid and Surface Properties, and Biochemistry. John Wiley and Sons, New York, USA.

Ioannidou, K., Krakowiak, K.J., Bauchy, M., Hoover, C.J., Masoero, E., Yip, S., Ulm, F.J., Levitz, P., Pellenq, R.J.M., Del Gado, E., 2016. Mesoscale texture of cement hydrates. Proceedings of the National Academy of Sciences of the United States of America 113, 2029–2034.

Jackson, M.D., Logan, J.M., Scheetz, B.E., Deocampo, D.M., Cawood, C.G., Marra, F., Vitti, M., Ungaro, L., 2009. Assessment of material characteristics of ancient concretes, Grande Aula, Markets of Trajan, Rome. J. Archaeol.Sci. 36 (11), 2481–2492.

Jackson, M.D., Landis, E.N., Brune, P.F., Vitti, M., Chen, H., Li, Q., Kunz, M., Wenk, H.R., Monteiro, P.J.M., Ingraffea, A.R., 2014. Mechanical resilience and cementitious processes in Imperial Roman architectural mortar. Proceedings of the National Academy of Sciences of the United States of America 111 (52), 18484–18489.

Jackson, M.D., 2014. Sea-water concretes and their material characteristics. In: Oleson, J.P. (Ed.), Building for Eternity. Oxbow Books, Philadelphia, USA, pp. 141–188.

Jackson, M.D., Chae, S.R., Mulcahy, S.R., Meral, C., Taylor, R., Li, P., Emwas, A.H., Moon, J., Yoon, S., Vola, G., Wenk, H.R., Monteiro, P.J.M., 2013. Unlocking the secrets of Al-tobermorite in Roman seawater concrete. American Mineralogist 98, 1669–1687.

Jennings, H.M., 2004. Colloid model of C-S-H and implications to the problem of creep and shrinkage. Materials and Structures 37, 59–70.

Jennings, H.M., 2008. Refinements to colloid model of C-S-H in cement: CM-II. Cement and Concrete Research 38, 275–289.

Keller, H., Plank, J., 2013. Mineralisation of $CaCO_3$ in the presence of polycarboxylate comb polymers. Cement and Concrete Research 54, 1–11.

Kingery, W., Vandiver, P., Prickett, M., 1988. The beginnings of pyrotechnology, Part II: production and use of lime and gypsum plaster in the pre-pottery neolithic Near East. Journal of Field Archaeology 15 (2), 219–244.

Kingery, W.D., 1960. Introduction to Ceramics. Wiley, New York, USA.

Kirkpatrick, R.J., Yarger, J.L., McMillan, P.F., Yu, P., Cong, X., 1997. Raman spectroscopy of C–S–H, tobermorite, and jennite. Advanced Cement Based Materials 5, 93–99.

Knauss, K.G., Wolery, T.J., 1988. The dissolution kinetics of quartz as a function of pH and time at 70 °C. Geochimica et Cosmochimica Acta 52, 43–53.

Kovačević, G., Persson, B., Nicoleau, L., Nonat, A., Veryazov, V., 2015. Atomistic modeling of crystal structure of $Ca_{1.67}SiH_x$. Cement and Concrete Research 67, 197–203.

Labbez, C., Jönsson, B., Woodward, C., Nonat, A., Delhorme, M., 2014. The growth of charged platelets. Physical Chemistry Chemical Physics 16, 23800–23808.

Lancaster, L., 2012. Ash mortar and vaulting tubes: agricultural production and the building industry in North Africa. In: Camporeale, S., Dessales, H., Pizzo, A. (Eds.), Les chantiers de construction de l'Italie et des provinces romaines: 3e rencontre. L'économie des chantiers (Paris, Ecole Normale Supérieure, 10-11 décembre 2009). Madrid, ES, pp. 145–160.

Manzano, H., Dolado, J.S., Ayuela, A., 2009. Aluminum incorporation to dreierketten silicate chains. Journal of Physical Chemistry B 113, 2832–2839.

Marchon, D., Juilland, P., Gallucci, E., Frunz, L., Flatt, R.J., 2017. Molecular and submolecular scale effects of comb-copolymers on tri-calcium silicate reactivity: toward molecular design. Journal of the American Ceramic Society 100, 817–841.

Margalha, M.G., Silva, A.S., Do Rosário Veiga, M., De Brito, J., Ball, R.J., Allen, G.C., 2013. Microstructural changes of lime putty during aging. Journal of Materials in Civil Engineering 25 (10), 1524–1532.

Marra, F., D'Ambrosio, E., Gaeta, M., Mattei, M., 2016. Petrochemical identification and insights on chronological employment of the volcanic aggregates used in ancient roman mortars. Archaeometry 58, 177–200.

Mascolo, G., Mascolo, M.C., Vitale, A., Marino, O., 2010. Microstructure evolution of lime putty upon aging. Journal of Crystal Growth 312 (16−17), 2363−2368.

Masoero, E., Delgado, E., Pellenq, R.J.M., Ulm, F.J., Yip, S., 2012. Nanostructure and nanomechanics of cement: polydisperse colloidal packing. Physical Review Letters 109, 155503.

Massazza, F., Testolin, M., 1983. Trimethylsilylation in the study of pozzolana-containing pastes. Il Cemento 80, 49−62.

Massazza, F., 2002. Properties and applications of natural pozzolanas. In: Bensted, J., Barnes, P. (Eds.), Structure and Performance of Cements. Spon Press, London, UK, pp. 326−352.

Matschei, T., Lothenbach, B., Glasser, F.P., 2007. The AFm phase in Portland cement. Cement and Concrete Research 37, 118−130.

McClellan, G.H., Eades, J.L., 1970. The textural evolution of limestone calcines. In: The Reaction Parameters of Lime, ASTM Special Publication 472. American Society for Testing and Materials, Philadelphia, USA, pp. 209−227.

Mertens, G., Snellings, R., Van Balen, K., Bicer-Simsir, B., Verlooy, P., Elsen, J., 2009. Pozzolanic reactions of common natural zeolites with lime and parameters affecting their reactivity. Cement and Concrete Research 39, 233−240.

Mogetta, M., 2015. A new date for concrete in Rome. Journal of Roman Studies 1−40.

Mollah, M.Y.A., Adams, W.J., Schennach, R., Cocke, D.L., 2000. A review of cement-superplasticizer interactions and their models. Advanced Cement Research 12, 153−161.

Moorehead, D.R., 1985. Cementation by the carbonation of hydrated lime. Cement and Concrete Research 16, 700−708.

Moropoulou, A., Bakolas, A., Aggelakopoulou, E., 2001. The effects of limestone characteristics and calcination temperature to the reactivity of the quicklime. Cement and Concrete Research 31, 633−639.

Nicoleau, L., 2013. The acceleration of cement hydration by seeding: influence of the cement mineralogy. ZKG International 1, 40−49.

Nonat, A., 2004. The structure and stoichiometry of C−S−H. Cement and Concrete Research 34, 1521−1528.

Ostwald, W., 1900. Über die vermeintliche Isomerie des roten und gelben Quecksilberoxyds und die Oberflächenspannung fester Körper. Z. Phys.Chem. 34 (1), 495−503.

Papatzani, S., Paine, K., Calabria-Holley, J., 2015. A comprehensive review of the models on the nanostructure of calcium silicate hydrates. Construction and Building Materials 74, 219−234.

Pecchioni, E., Fratini, F., Cantisani, E., 2008. Le malte antiche e moderne tra tradizione e innovazione. Patron Editore, Bologna, IT.

Pegado, L., Labbez, C., Churakov, S.V., 2014. Mechanism of aluminium incorporation into C−S−H from ab initio calculations. Journal of Materials Chemistry 2, 3477−3483.

Plinio il Vecchio, 1984. Naturalis Historia. Giardini Editore, Pisa, IT.

Provis, J.L., Lukey, G.C., van Deventer, J., 2005. Do geopolymers actually contain nanocrystalline zeolites? A reexamination of existing results. Chemistry of Materials 17, 3075−3085.

Provis, J.L., van Deventer, J.S.J., 2014. Alkali Activated Materials, State-of-the-art Report, RILEM TC 224-AAM. Springer, Dordrecht, the Netherlands.

Richardson, I.G., 2008. The calcium silicate hydrates. Cement and Concrete Research 38, 137−158.

Richardson, I.G., Brough, A.R., Brydson, R., Groves, G.W., Dobson, C.M., 1993. Substituted calcium silicate hydrate (C-S-H) gels as determined by ^{29}Si and ^{27}Al NMR and EELS. Journal of the American Ceramic Society 76, 2285−2288.

Rodriguez-Navarro, C., Benning, L.G., 2013. Control of crystal nucleation and growth by additives. Elements 9, 203−209.

Rodriguez-Navarro, C., Hansen, E., Ginell, W.S., 1998. Calcium hydroxide crystal evolution upon aging of lime putty. Journal of the American Ceramic Society 81 (11), 3032−3034.

Rodriguez-Navarro, C., Ruiz-Agudo, E., Luque, A., Rodriguez-Navarro, A.B., Ortega-Huertas, M., 2009. Thermal decomposition of calcite: mechanisms of formation and textural evolution of CaO nanocrystals. American Mineralogist 94 (4), 578−593.

Ruiz-Agudo, E., Rodriguez-Navarro, C., 2010. Microstructure and rheology of lime putty. Langmuir 26, 3868–3877.
Schiele, E., Berens, L.W., 1976. In: Tecniche, E.T. (Ed.), La calce. Calcare, calce viva, idrato di calce. Milano, IT.
Scrivener, K.L., Crumbie, A.K., Laugesen, P., 2004. The interfacial transition zone (ITZ) between cement paste and aggregate in concrete. Interface Science 12, 411–421.
Serry, M.A., Taha, A.S., El-Hemaly, S.A.S., El-Didamony, H., 1984. Metakaolin-lime hydration products. Thermochimica Acta 79, 103–110.
Shaw, J.W., 1973. Minoan architecture: materials and techniques. Annuario della Scuola Archeologica di Atene 49, 883–889.
Shvab, I., Brochard, L., Manzano, H., Masoero, E., 2017. Precipitation mechanisms of mesoporous nanoparticle aggregates: off-lattice, coarse-grained, kinetic simulations. Crystal Growth and Design 17, 1316–1327.
Skinner, L.B., Chae, S.R., Benmore, C.J., Wenk, H.R., Monteiro, P.J.M., 2010. Nanostructure of calcium silicate hydrates in cements. Physical Review Letters 104, 195505.
Snellings, R., Mertens, G., Elsen, J., 2012. Supplementary cementitious materials. Reviews in Mineralogy and Geochemistry 74 (1), 211–278.
Sowoidnich, T., Rachowski, T., Rössler, C., Völker, A., Ludwig, H.M., 2015. Calcium complexation and cluster formation as principal modes of action of polymers used as superplasticizer in cement systems. Cement and Concrete Research 73, 42–50.
Soyer-Uzun, S., Chae, S.R., Benmore, C.J., Wenk, H.R., Monteiro, P.J.M., 2012. Compositional evolution of calcium silicate hydrate (C–S–H) structures by total X-ray scattering. Journal of the American Ceramic Society 95, 793–798.
Stark, J., Wicht, B., 1999. Zur Historie des Gipses. ZKG (Zement, Kalk, Gips) 52 (10), 527–533.
Stern, K.H., 1954. The Liesegang phenomenon. Chemical Reviews 54, 79–99.
Sun, J., Shi, H., Qian, B., Xu, Z., Li, W., Shen, X., 2017. Effects of synthetic C–S–H/PCE nanocomposites on early cement hydration. Construction and Building Materials 140, 282–292.
Suraneni, P., Flatt, R.J., 2015. Micro-reactors to study alite hydration. Journal of the American Ceramic Society 98, 1634–1641.
Takemoto, K., Uchikawa, H., 1980. Hydratation des ciments pouzzolaniques. In: Proceedings of the 7th International Congress on the Chemistry of Cement, vols. I, IV. Editions Septima, Paris, FR, pp. 1–21.
Tavasci, B., 1947. Struttura della Malta di cake e pozzolana di Segni. Il Cemento 43, 106–108.
Taylor, H.F.W., 1986. Proposed structure for calcium silicate hydrate gel. Journal of the American Ceramic Society 69, 464–467.
Taylor, H.F.W., 1997. Cement Chemistry. Thomas Telford, London, UK.
Theodoridou, M., Ioannou, I., Philokyprou, M., 2013. New evidence of early use of artificial pozzolanic material in mortars. Journal of Archaeological Science 40 (8), 3263–3269.
Thomas, J.J., Jennings, H.M., Chen, J.J., 2009. Influence of nucleation seeding on the hydration mechanisms of tricalcium silicate and cement. Journal of Physical Chemistry C 113, 4327–4334.
Tomazic, B., Mohanty, R., Tadros, M., Estrin, J., 1986. Crystallization of calcium hydroxide from aqueous solution: ii. Observation of growth, morphology and secondary nucleation. Journal of Crystal Growth 75, 339–347.
Türker, P., Yeginobali, A., 2003. Comparison of hydration products of different pozzolanic systems. In: Proceedings of the 25th International Conference on Cement Microscopy. Richmond, USA, pp. 1–9.
U.S. Geological Survey, 2017. Mineral Commodity Summaries.
Valentini, L., Artioli, G., Voltolini, M., Dalconi, M.C., 2012. Multifractal analysis of calcium silicate hydrate (C–S–H) mapped by x-ray diffraction microtomography. Journal of the American Ceramic Society 95, 2647–2652.

Valentini, L., Favero, M., Dalconi, M.C., Russo, V., Ferrari, G., Artioli, G., 2016. Kinetic model of calcium-silicate hydrate nucleation and growth in the presence of PCE superplasticizers. Crystal Growth and Design 16, 646−654.

van Driessche, A.E.S., Kellermeier, M., Benning, L.G., Gebauer, D., 2017. New Perspectives on Mineral Nucleation and Growth. From Solution Precursors to Solid Materials. Springer, Cham, Switzerland.

Vitruvio, M.P., 1997. De Architectura. Einaudi, Torino, IT.